SAXS Studies of Polymer Melting: Models for Surface Melting, Sequential Melting, and Stack Melting

Buckley Crist

Department of Materials Science & Engineering, Northwestern University, Evanston, Illinois 60208-3108

Received February 14, 2003; Revised Manuscript Received April 17, 2003

ABSTRACT: Melting of semicrystalline polymers typically occurs over a temperature range of 10 °C or more, throughout which the long period L increases by 50%−100%. Less recognized is the evolution of the small-angle X-ray scattering (SAXS) pattern from peaked to monotonic before the final stages of melting. These two features are considered with SAXS patterns calculated for basal surface melting, for sequential melting by increasing thickness of randomly placed crystals, and for melting of separate stacks of lamellar crystals having different periods. Calculated intensities are further analyzed by the correlation function $\gamma(r)$ and the interface distribution function $G(r)$. Neither surface melting nor sequential melting can account for the commonly observed increase in L, although the sequential mechanism provides monotonic scattering from single lamellae as melting is completed. Stack melting can display an increase in L, but not a conversion to monotonic scattering. A reasonable conclusion is that most melting is accompanied by extensive reorganization by melting and recrystallization or by lamellar thickening. Sequential melting is favored in systems with very stable crystals that are resistant to reorganization.

Introduction

It has been known for more than 70 years that crystals formed by flexible or semirigid polymer molecules typically melt over a range of tens of degrees or more, and that the melting range is dependent on crystallization conditions. From such observations van Rossem and Lotichius[1] first proposed in 1929 that crystal size was responsible for variable melting temperatures in natural rubber. Some two decades later, Flory[2] formulated a quantitative relation between crystal thickness c and melting (or equilibrium crystallization) temperature. The subsequent discovery that polymers crystallize with lamellar habits led to the generally accepted Gibbs−Thomson relation for melting temperature T_m being inversely related to crystal thickness c, with the caveat that thin metastable crystals may rapidly reorganize and melt again at a higher temperature.[3] A host of experimental techniques have been employed to study the rather diffuse transition of polymers from the semicrystalline state to the liquid state, the most common being differential scanning calorimetry (DSC) which, with the aid of certain assumptions, can supply estimates of the thickness of crystals that melt.[4] Small-angle X-ray scattering (SAXS) to follow structural changes during polymer melting was first done by Belbéoch and Guinier[5] in 1959, who addressed the fusion of branched (high pressure) polyethylene. The authors of that seminal work associated the peaked SAXS pattern with a periodic arrangement of lamellar crystals. They further showed that heating from room temperature to 96 °C, just below $T_m = 103$ °C, increased the average long period by more than 30% and increased the intensity of the interference peak by more than 100%. At still higher temperatures, the intensity passed through a maximum and decreased rapidly to zero at T_m.

Scores of SAXS studies of polymer melting have been reported over the subsequent decades. Despite renewed interest spurred by the availability of synchrotron X-ray sources, our knowledge of the melting process has advanced surprisingly little. Three fundamentally different mechanisms have been proposed, all of which are predicated on a morphology of stacks of lamellar crystals separated by amorphous domains. One model relies on *sequential melting* of individual lamellar crystals within a stack according to stability. The second model is a variation in which separate stacks of thinner, less stable crystals melt first. Sequential melting of crystals according to size was first proposed by Bebléoch and Guinier[5] to account intensity changes during the melting transition, and was considered somewhat later by O'Leary and Geil[6] to explain the increase in long period. Pope and Keller[7] seem to have been the first to mention the melting of entire stacks at different temperatures (*stack melting*). The third mechanism, in which all lamellar crystals melt simultaneously and partially from the large basal surfaces (*surface melting*), was advanced by Fischer and his colleagues.[8] While all of these melting schemes account for a broad transition range, each has different effects on the SAXS pattern. In this paper the general relation between melting and SAXS for semicrystalline polymers is considered first. Then are presented calculated SAXS patterns for surface melting, sequential melting and stack melting which are compared to experimental SAXS patterns reported by others. The goal of this work is to investigate and interpret the connection between polymer melting and SAXS, as opposed to assigning specific melting mechanisms.

Melting and SAXS: General Data

SAXS patterns from semicrystalline polymers are almost always analyzed in terms of a one-dimensional model of stacked lamellar crystals separated by amorphous domains. Crystals are assumed to be flat, parallel and of effectively infinite width. The preferred structural model has sharp interfaces between crystalline and amorphous regions; the unwanted effects of transition zones are usually removed prior to quantitative analysis.[9,10] Information on the structure is inferred from the

10.1021/ma030113d CCC: $25.00
Published on Web 06/03/2003

shape of the scattering pattern as well as the absolute (or relative) intensity.

Let the experimental pattern for an isotropic sample be $I_{iso}(s)$, where the magnitude of the scattering vector is $s = 2(\sin\theta)/\lambda$, θ being half the scattering angle and λ the wavelength. This intensity is modified to that for the scattering model, a one-dimensional stack of lamellar crystals, as follows:

$$I(s_1) = 2\pi s^2 I_{iso}(s) \tag{1}$$

The scattering vector of magnitude s_1 is understood to be parallel to the stacking direction or normal to crystalline-amorphous interfaces. Integration of eq 1 gives the invariant Q (electron^2/m^3):

$$Q = \int_{-\infty}^{\infty} I(s_1)\, ds_1 = 4\pi \int_0^{\infty} s^2 I_{iso}(s)\, ds \tag{2}$$

For a two-phase crystalline-amorphous model with volume fraction of crystals n and electron density difference $\Delta\rho_e$ (electron/m^3), the invariant is equal to[11,12]

$$Q = V\varphi_{st}\varphi(1-\varphi)\Delta\rho_e{}^2 \tag{3}$$

The irradiated sample volume is V, φ_{st} is the (volume) fraction of the sample that gives rise to the observed SAXS pattern, and φ is the crystalline fraction within the stack, sometimes referred to as the local or one-dimensional crystallinity.

At this point it is instructive to consider two examples of SAXS studies of melting. Data in Figure 1 are from Denchev et al.[13] for experiments on poly(ethylene naphthalene 2,6-dicarbonate), PEN. Samples were quenched to the glassy state, then crystallized isothermally at 165 °C (a) or at 240 °C (b). Experimental SAXS patterns $I_{iso}(q)$ were recorded at the indicated temperatures while heating at 10 °C/min; here $q = 2\pi s$ is another measure of the size of the scattering vector. At selected temperatures are indicated t, the fraction of original crystals that have melted, as estimated from wide-angle X-ray diffraction. The small signal for completely molten polymer ($t = 1$) is parasitic scattering from the beamstop. Results in Figure 1a are representative of many SAXS melting experiments. The position of the interference peak clearly shifts to smaller values of q (or s) and the peak intensity of $I_{iso}(s)$ increases about 7-fold on heating from 170 to 255 °C. While half of the original crystals are present at $T = 262$ °C ($t = 0.5$), the SAXS pattern displays no maximum; it is unclear whether the peak has shifted behind the beamstop or if the interference peak has simply decayed. Further heating leads to continuous decrease of intensity until final melting at $T = 274$ °C. The behavior shown by PEN (b), crystallized at the higher temperature, is quite different, and has been reported only occasionally. Structural changes are obviously confined to the smaller temperature interval between 240 °C and final melting at 274 °C. Note particularly that the interference peak persists near its original position, even when $t = 0.5$ at $T = 270$ °C, while intensity at the lowest measurable q increases. The observed pattern is devoid of a maximum for $T >$ 270 °C, and decreases in intensity until final melting, again at 274 °C.

Invariant or intensity changes are considered first. On melting, φ_{st} may remain constant (sequential or surface melting) or may decrease (stack melting). For either sequential or surface melting, the product $\varphi(1-\varphi)$ eventually approaches zero, but it may go through a maximum if the initial stack crystallinity φ_o is greater than 0.5. From a practical perspective, $\varphi(1-\varphi)$ changes only trivially (from 0.24 to 0.25 and back to 0.24) as stack crystallinity drops from 0.6 to 0.4, so the invariant is insensitive to structure changes in this range. Increased temperature enhances the electron density difference $\Delta\rho_e$; from the thermal expansion coefficients of crystalline and amorphous polyethylene, $\Delta\rho_e{}^2$ and hence Q are expected to increase by about 30% over an interval of 100 °C if structure is otherwise unchanged. The same difference in expansion coefficients would cause the stack crystallinity φ to drop by ~5% (relative) over the same 100 °C range, e.g., from $\varphi = 0.50$ to $\varphi = 0.48$. While $Q(T)$ or an approximation thereof is reported in many SAXS studies of melting, the positive temperature dependence of $\Delta\rho_e{}^2$ must be accounted for to establish whether the structure-dependent part of the invariant displays a maximum with respect to temperature. Fougnies et al.[14] have demonstrated a straightforward method for evaluating $\Delta\rho_e{}^2(T)$ and subsequently extracting $V\varphi_s\varphi(1-\varphi)$ from $Q(T)$. Absent a step of this sort, one can only conclude that the decrease of $Q(T)$ to zero as T_m is approached indeed reflects the final stages of melting.

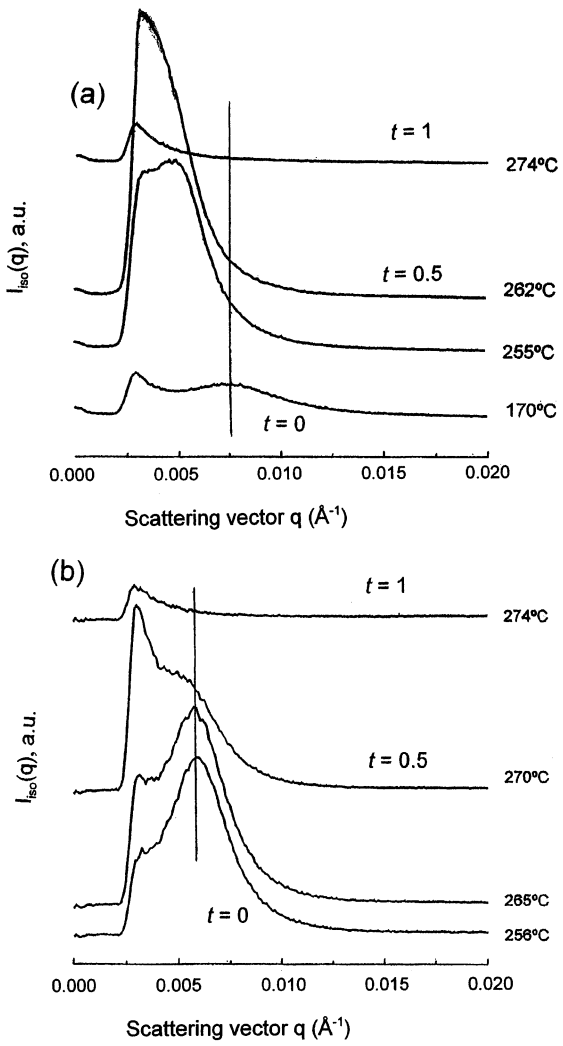

Figure 1. Experimental SAXS patterns of PEN during melting. Sample a was crystallized at 165 °C; sample b was crystallized at 240 °C. Measurement temperature is indicated, as is t, the fraction of original crystals melted. After Denchev et al.[13]

Peak intensity is a different matter, depending on the shape of the pattern in addition to invariant-related factors considered above. One aspect seems to have been overlooked. If the average period L is increased (for whatever reason) by 50% while all other structural features are fixed, the peak in $I(s_1)$ will increase by 50% simply because the s_1 range of the pattern has been compressed. Combining this with the 30% increase from thermal expansion difference, the Lorentz corrected peak intensity would nearly double over a 100 °C range if L increased by 50%. Even larger changes are expected for the experimental $I_{iso}(s)$ in eq 1; here a 50% increase in L will cause the peak intensity to grow to 3.4 times its original value (neglecting any changes in $\Delta\rho_e^2$). This effect alone can account for nearly half of the intensity change seen in Figure 1a on heating PEN from 170 to 255 °C. Be clear, however, that this tells us nothing about why L increased by 50%.

Considerably more information about melting is conveyed by the *shape* of the SAXS pattern. At lower temperatures there is an interference maximum in $I(s_1)$ at $s_1 = s_1^*$ that reflects the periodicity of the stack of lamellar crystals. (This is seen as a peak in the experimental $I_{iso}(q)$ in Figure 1 at slightly smaller values of $s = q/2\pi$.) As T_m is approached by heating, the peaked pattern (with a peak or conspicuous shoulder at $s_1 > 0$) evolves to a monotonic one that decreases smoothly from the maximum at $s_1 = 0$. This very important aspect of melting and SAXS has often been overlooked. Quite unambiguously, the conversion from a peaked to a monotonic SAXS pattern shows that isolated lamellae are present at the end of the melting range, an effect observed for polyethylene,[15] sydiotactic polypropylene[16] and poly(3-hydroxybutyrate).[17] Such behavior is consistent with the sequential melting mechanism, which in some sense is the reverse of crystallization that starts with the formation of isolated lamellar crystals.[16,18−20] Regarding this monotonic scattering, there is an unwarranted notion that the Lorentz-corrected intensity (eq 1) must go to zero at $s_1 = 0$, which is the case only for a perfect lattice (see eq 8 below). If SAXS data are manipulated to force this incorrect behavior,[10,21,22] then the evolution of the pattern from peaked to monotonic will not be observed, and the invariant will appear to decrease more abruptly than it actually does. The raw experimental scans in Figure 1, which have not been processed in any way, clearly show patterns that appear to be more monotonic at higher temperatures.

Virtually all SAXS studies of polymer melting have been more concerned with the evolution of structural sizes as macroscopic crystallinity decreases. Here are summarized briefly the methods by which various dimensions are evaluated from SAXS. One measure of average stack periodicity is from Bragg's law applied to the position of interference maximum $I(s_1 = s_1^*)$ which gives $L_B = 1/s_1^*$. A popular alternative uses the normalized one-dimensional correlation function:[23]

$$\gamma(r) = \frac{2}{Q}\int_0^\infty I(s_1)\cos(2\pi s_1 r)\,ds_1 \qquad (4)$$

The period of the one-dimensional structure is given by the position of the first maximum (beyond the origin) of $\gamma(r)$ when $r = r^* = L_\gamma$. Additionally, the value of r at which $\gamma(r)$ first becomes zero is used to establish l_2, the *smaller* of the two phase thicknesses. The same quantity can be determined from the most negative value of $\gamma(r)$ and L_γ, provided the correlation function is flat in that region, a condition most easily met for large or small values of φ.[23] The larger phase thickness is obtained by difference, i.e., $l_1 = L_\gamma - l_2$, and independent information is needed to establish whether the larger thickness l_1 is for crystalline or amorphous domains. Fulcher et al.[24] were the first to evaluate phase thicknesses and stack crystallinity during melting by fitting models with appropriate l_1 and l_2 to the experimental correlation function given by eq 4. More recent studies usually extract some average L_γ, l_2, and l_1 from direct inspection of $\gamma(r)$, as outlined above.

The third method of analysis is based on the one-dimensional interface distribution function[25]

$$G(r) = 8\pi^2\int_0^\infty [K_P - s_1^2 I(s_1)]\cos(2\pi s_1 r)\,ds_1 \qquad (5)$$

where $K_P = \lim_{s_1\to\infty} s_1^2 I(s_1)$ is the Porod constant for a one-dimensional, two phase structure with sharp interfaces. $G(r)$ can also be evaluated as the second derivative of $\gamma(r)$. The first maximum in $G(r)$ is the most probable value of the *smaller* of the two phase thicknesses l_2, and $G(r)$exhibits a negative extremum at $r = L_G$. As with $\gamma(r)$, the larger phase thickness is obtained by difference as $l_1 = L_G - l_2$. The present author has recently considered the significance and reliability of period L, phase thickness l, and phase volume fraction l/L obtained by these methods.[26] In particular, it was found that a second maximum in $G(r)$, if present, is often a very unreliable estimate of the larger thickness l_1.

SAXS/melting experiments have been reviewed in a recent article by Crist.[27] It is commonly observed that the period L (either L_B, L_γ, or L_G) increases by 50%−100% during heating to T_m; such behavior can be inferred from the intensity maxima in Figure 1a. From analyses, usually by the correlation function $\gamma(r)$, the thickness of one phase is seen to increase strongly during melting, while the other phase grows moderately or may even decrease. A pattern was noticed with this behavior;[27] for polymers of low overall crystallinity, the larger thickness l_1 increases strongly during melting, while for polymers with large initial crystallinity, the smaller thickness l_2 has the dominant temperature dependence. These observations can be reconciled if the average amorphous layer thickness—large for low crystalline polymers and small for those of high crystallinity—increases during melting. While it is acknowledged assigning the thickness dimensions l_1 and l_2 to either crystalline or amorphous phases entails uncertainty,[28] the pattern mentioned above is a robust one. Given that the average amorphous layer thickness $\bar{a}$ does increase during melting, there are at least two mechanisms, introduced above, to achieve this change. Sequential melting of crystals of increasing size was proposed in the pioneering study by Belbéoch and Guinier[5] and many times since. The basic idea is that complete melting of some randomly placed crystals within the stack increases the average amorphous thickness $\bar{a}$. For example, melting half of the crystals ($t = 0.5$) would increase $\bar{a}$ by about three times and increase the average period of a stack by about two times. (It will be shown below that SAXS experiments do not reveal these increases in *average* dimensions.) Fischer[8] and coworkers were more concerned with the increase in peak intensity on heating, and proposed that amorphous domains between all lamellar crystals grow with increasing $T < T_m$. By this process the lamellar crystals are gradually converted to the liquid state by surface

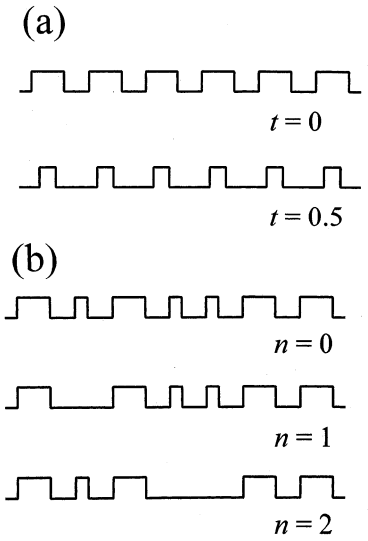

Figure 2. Melting of lamellar stacks represented by density profiles. (a) Schematic of surface melting for transformation index $t = 0.5$. (b) Schematic of sequential melting of thin crystals in groups of zero ($n = 0$), one ($n = 1$), and two ($n = 2$). Relative amounts of such sequences vary with t according to eq 10.

melting. While surface melting has current adherents,[29,30] that process occurs at essentially constant L, with the increase in $\bar{a}$ being compensated for by a decrease in average crystal thickness $\bar{c}$. That behavior is inconsistent with commonly observed 50%−100% increases in L during melting (Figure 1a), but is in accord with the fairly rare instances when L is nearly constant (Figure 2b). The concept of stack melting has evolved into the "dual lamellar stacks" model, in which physically separate stacks containing thin and thick lamellae melt at low and high temperatures, respectively. The inference of two stack populations comes mainly from analyses of SAXS patterns during isothermal crystallization and subsequent melting.[31,32] The increase in apparent L during heating is said to result from first melting those stacks with the small period, leaving the population with the larger period to scatter before final melting.[13]

The transformation of lamellar stacks to the liquid state by surface melting and by sequential melting are considered in detail in this paper. SAXS patterns are calculated and analyzed, as in experiment, by the appearance of $I(s_1)$ and by analyses of the derived functions $\gamma(r)$ and $G(r)$. Stack melting is considered briefly. The principal result is that neither surface melting nor sequential melting can cause the 50%−100% increase in L that is observed in many SAXS/melting experiments. While large increases in L may derive from stack melting, that mechanism does not account for the enhanced intensity seen in Figure 1a. In such instances, the most logical conclusion is that there is significant rearrangement of the lamellar microstructure during melting. The infrequently seen behavior in Figure 1b is consistent with sequential melting. A key signature is the weakening interference maximum, essentially unchanged in position, being overwhelmed by increased intensity at the lowest angles.

Scattering Model

As in previous work, the general paracrystalline model of Hermans,[33] popularized by Hosemann and Bagchi, is employed.[34] The semicrystalline polymer is represented by lamellar crystals having thickness distribution $H(c)$ separated by amorphous regions characterized by thickness distribution $h(a)$. In the stack there is no correlation between the size of a crystal and the thicknesses of the neighboring amorphous regions. Scattering is evaluated for a stack of N crystals of effectively infinite height Z, wherein each lamella has a basal surface area A:

$$I(s_1) = \frac{NA\Delta\rho_e^{\,2}}{2\pi^2 s_1^{\,2}} \mathrm{Re}\left[\frac{(1 - F_c)(1 - F_a)}{1 - F_c F_a}\right] \qquad (6)$$

All information about stack periodicity and phase thicknesses are contained in F_c and F_a, the respective Fourier transforms of $H(c)$ and $h(a)$. The one-dimensional intensity $I(s_1)$ has been integrated over reciprocal space dimensions transverse to the stacking direction, and it has units of electron^2/m^2.

Gaussian probability density functions are employed for mathematical convenience to describe the *original* phase thicknesses (prior to any melting). For the crystalline phase one writes:

$$H_o(c) = \frac{1}{\sigma_{co}\sqrt{2\pi}} \exp[-(c - c_o)^2/2\sigma_{co}^{\,2}]$$

$$F_{co} = \exp[-2\pi^2 s_1^{\,2}\sigma_{co}^{\,2}] \exp[-2\pi i s_1 c_o] \qquad (7)$$

Analogous expressions are used for *original* amorphous functions $h_o(a)$ and F_{ao}. Variables are mean thickness c_o (and a_o) and variance σ_{co}^2 (and σ_{ao}^2). The original period is $x_o = c_o + a_o$, original stack crystallinity is $\varphi_o = c_o/x_o$ and amorphous fraction is $1 - \varphi_o = a_o/x_o$. Reference is made to the reduced standard deviations $g_c = \sigma_c/\bar{c}$ or $g_a = \sigma_a/\bar{a}$ for the phases and $g_x = [\varphi^2 g_c^{\,2} + (1 - \varphi)^2 g_a^{\,2}]^{1/2}$ for the structural period. For all cases $g_x = 0.2$ for the original (unmelted) structures, and $H_o(c)$ and $h_o(a)$ are defined so that the *original* g_c and g_a equal one another.

Partial melting is expressed as the fraction t of the *original* crystals that have transformed to the liquid state; t evolves from zero to one as the melting process goes from beginning to end. When considering sequential melting or surface melting, for each value of t are evaluated a modified crystal thickness distribution $H(c)$ and amorphous thickness distribution $h(a)$, from which are calculated the Fourier transforms F_c and F_a, and hence $I(s_1)$ with eq 7, the correlation function $\gamma(r)$ with eq 4, and the interface distribution function $G(r)$ with eq 5. Stack melting is treated differently. The unmelted sample consists of stacks of different average period (but the same stack crystallinity φ_o and phase statistics g_c and g_a) with weighted populations. Partial melting here involves removing the population of one or more stacks to increase t. The structure of the surviving stacks is unchanged.

Before considering the effects of melting on SAXS, some relations between stack structure and the intensity function $I(s_1)$ are reviewed.[27,33] Readers are certainly aware that $I(s_1)$ displays interference maxima near $s_1 = j/x$, $j = 1, 2, \ldots$, and that higher order maxima are suppressed by stack disorder g_x. Often overlooked is that fact that (Lorentz corrected) intensity at $s_1 = 0$

is proportional to disorder within the stack:

$$I(0) = NA\Delta\rho_e^2[\varphi^2\sigma_a^2 + (1 - \varphi^2)^2\sigma_c^2] \qquad (8)$$

As mentioned above, forcing $I(0)$ to zero removes authentic information content from the pattern and reduces the invariant. Equation 8 does not apply when stack periodicity has been destroyed by nearly complete sequential melting. In that case one observes scattering from a few isolated lamellae and $I(0) = NA\Delta\rho_e^2\overline{c^2}$. At the other end of the scattering domain is the Porod constant:

$$K_p = \frac{\Delta\rho_e^2}{4\pi^2} S$$

Letting the surface area S associated with the stack be $S = 2NA$, one obtains

$$K_p = \frac{NA\Delta\rho_e^2}{2\pi^2} \qquad (9)$$

Note that the Porod constant is proportional to the number N of lamellae per stack.

Intensity $I(s_1)$ is calculated for various extents of transformation t and expressed as $I(s_1)/N_oA\Delta\rho_e^2$, where N_o is the *original* number of lamellae in a stack. For sequential and surface melting, only the internal structure of the stack changes with t. One stack is representative of the entire sample, and the "structure fraction" $\varphi_{st} = 1$. While N is allowed to change as appropriate, the area A is assumed to be constant. This normalized intensity is manipulated to obtain the correlation function $\gamma(r)$ (eq 4) and interface distribution function $G(r)$ (eq 5 without the factor $8\pi^2$). The magnitude of the scattering vector s_1 is in units of $1/x_o$, and distances are in units of x_o. Stack melting is treated by a different procedure that is described later.

Surface Melting

Surface melting is illustrated in Figure 2a; each crystal, regardless of initial thickness, loses a fraction $t/2$ to each of two neighboring amorphous layers. The number of lamellae $N = N_o$, the average period $\bar{x} = x_o = c_o + a_o$ and variances of crystal thickness σ_c^2 and amorphous thickness σ_a^2 are constant throughout this melting process, while the average phase thicknesses become $\bar{c} = c_0 - c_0t$ and $\bar{a} = a_0 + c_0t$. Intensity and corresponding correlation and interface distribution functions are given in Figures 3−5. Calculations are restricted to $t \leq 0.6$, because the crystal distribution $H(c)$ acquires a significant fraction of negative thicknesses as the mean $\bar{c}$ decreases while the variance σ_c^2 is constant.

For the illustrated case where initial crystallinity $\varphi_o = 0.75$, there is a maximum in peak intensity as t passes through 0.33 that corresponds to stack crystallinity $\varphi = 0.5$. Be reminded that in a real experiment, where contrast factor $\Delta\rho_e^2$ increases with temperature, the intensity is enhanced at larger t. Surface melting preserves the stack throughout the transition; overall stack disorder measured by $I(0)$ remains small as the variances σ_c^2 and σ_a^2 are fixed (see eq 8).

The average period $\bar{x} = x_0$ is unchanged by surface melting, and one sees that L_B, L_γ, and L_G measured by scattering are nearly constant. The periods summarized in Table 1 indicate an apparent increase of less than 5% from $I(s_1)$ and $\gamma(r)$, and a decrease of about the same size from $G(r)$. These subtle changes are an order of magnitude less than the increases seen in most experi-

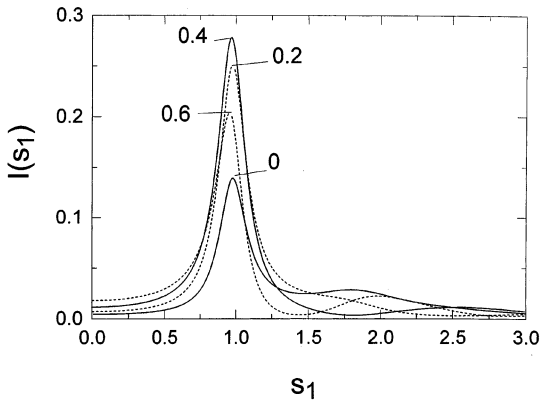

Figure 3. Intensity $I(s_1)$ of lamellar stack with initial crystallinity $\varphi_o = 0.75$ for surface melting fractions t indicated. Period $L_B = 1/s^*$ is presented in Table 1.

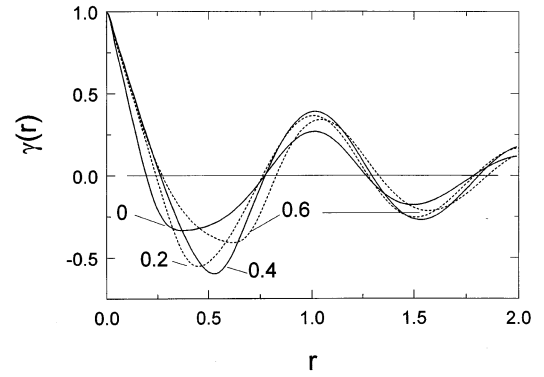

Figure 4. Correlation function $\gamma(r)$ for surface melting, $\varphi_o = 0.75$ as in Figure 1. Position of first maximum is period L_γ, while r at which $\gamma(r) = 0$ leads to crystallinity $\varphi_{\gamma o}$, and depth of first minimum gives $\varphi_{\gamma min}$. See Table 1.

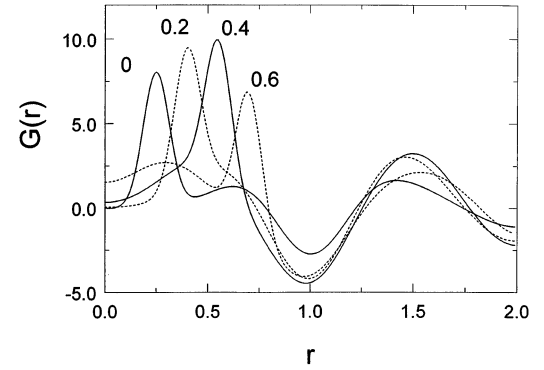

Figure 5. Interface distribution function $G(r)$ for surface melting, $\varphi_o = 0.75$ as in Figure 1. Position of minimum is period L_G. Positive peak shifting to larger r with larger t is amorphous distribution $h(a)$; crystalline $H(c)$ is observable near $r = 0.3$ for $t = 0.6$.

Table 1. Surface Melting for Lattice with Initial Crystallinity $\varphi_0 = 0.75$

t	$\bar{x}$	L_B	L_γ	L_G	φ	$\varphi_{\gamma 0}$	$\varphi_{\gamma min}$	φ_G
0	1.00	1.02	1.02	1.01	0.75	0.72	0.75	0.75
0.2	1.00	1.03	1.01	0.99	0.60	0.61	0.64	0.61
0.4	1.00	1.04	1.02	0.98	0.45	*a*	0.37	0.46
0.6	1.00	1.05	1.05	0.97	0.30	*a*	0.29	0.31

[a] Equation returns a complex result.

ments, and are in part artifacts that derive from the growing presence of negative c at large t. Nevertheless, all derived quantities in Table 1 are basically sound, as the intensities in Figure 3 conform to analytical expectations for intercept $I(0)$ (eq 8), Porod constant K_p (eq 9) and invariant Q (eq 3). That is not the case for $t >$ 0.6. Also given in Table 1 are stack crystallinity φ and measures thereof from $\gamma(r)$ and $G(r)$. Two values are obtained from the correlation function; that from the first zero of $\gamma(r)$ is $\varphi_{\gamma 0}$, while that from the depth of the minimum is $\varphi_{\gamma \min}$. In this example at least, crystallinity estimates from $\varphi_{\gamma \min}$ are superior to those from $\varphi_{\gamma 0}$. Both correlation function methods face difficulty when the stack crystallinity is near 0.5. The interface distribution function in Figure 5, on the other hand, clearly reflects surface melting through the positively shifting peak corresponding to the evolution of amorphous thickness distribution $h(a)$ with increasing t. The smaller peak seen for $t = 0.6$ is for the crystal $H(c)$ centered at $c_o(1 - t) = 0.45$. Estimates of crystallinity φ_G are in excellent accord with φ.

To summarize, surface melting leaves the average period $\bar{x}$ unchanged. The lattice persists throughout the melting process, and there is no pronounced intensity growth at low s_1. Integrated and peak intensities (ignoring thermal expansion) are proportional to $\varphi(1 - \varphi) = \varphi_o(1 - t)(1 - \varphi_o(1 - t))$. Samples with initial crystallinity $\varphi_o > 0.5$ will display an intensity maximum with respect to the melting parameter t. All measures of stack period are very close to the true, constant value. Crystallinity estimates from the correlation function are more reliable if the minimum of $\gamma(r)$ is used. The interface distribution function $G(r)$ displays the changing thickness distributions, particularly amorphous $h(a)$, with near perfect accuracy.

Sequential Melting

Consider now an alternative mechanism by which the thinner crystals within a stack melt completely while thicker ones are unaffected. This process is considered here in detail, because it has most often been invoked to explain the increase in L over the melting range, from the earliest quantitative analyses of Fulcher and Brown[24] until the present.[35] The transformation index t is here the fraction of crystals in the initial distribution $H_o(c)$ that have melted. How does one describe the lattice in this case? The answer, of course, lies in the modified distributions for the lamellae $H(c)$ and amorphous gaps $h(a)$. The general paracrystalline model requires there be no correlation between crystal thickness and relative position in the lattice, hence the melted crystals are distributed randomly. For a particular t, all crystals of thickness $c \le c_m$ have melted, and the resulting normalized crystal distribution $H(c)$ with mean $\bar{c} > c_o$ is defined for the range $c_m < c < \infty$. Also note that the melted lamellae are described by a distribution of transformed crystals $H_t(c)$ with mean $c_t \le c_o$ over the range $0 \le c \le c_m$. $H(c)$ is shown in Figure 6a for $t = 0$ and $t = 0.6$ for the case when initial crystallinity $\varphi_o = 0.75$. The required Fourier transform F_c for use in eq 6 is evaluated numerically.

The amorphous thickness distribution $h(a)$ that develops during sequential melting is more complex. In a stack that may be partially melted ($t \ge 0$), one starts with an amorphous layer next to a crystal. If the original crystal that bounded the other side of the amorphous layer is unmelted, that particular layer is unmodified

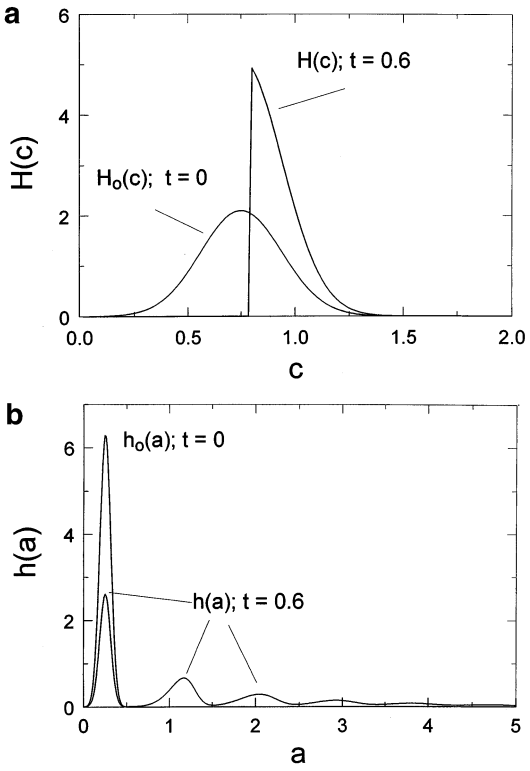

Figure 6. (a) Crystal thickness distributions for stack with initial crystallinity $\varphi_o = 0.75$. $H_o(c)$ with mean $c_o = 0.75$ is for no melting, $t = 0$. $H(c)$ with mean $\bar{c} = 0.93$ develops after sequential melting to $t = 0.6$; the thickest melted crystal is $c_{max} = 0.78$. (b) Amorphous thickness distributions for stack with initial crystallinity $\varphi_o = 0.75$. $h_o(a)$ with mean $a_o = 0.25$ is for no melting, $t = 0$. $h(c)$ with mean 1.50 develops after sequential melting to $t = 0.6$. The maxima in $h(a)$ correspond to $n = 0$, $n = 1$, $n = 2$, etc.

and corresponds to the original average thickness a_o indicated in the $n = 0$ line of Figure 2b. When *one* bounding lamellar crystal melts, the amorphous region has a size equal to the sum of the melted crystal plus the two flanking amorphous layer thicknesses, as illustrated by the $n = 1$ sketch in Figure 2b. The average amorphous gap size so created is $c_t + 2a_o$. Melting $n = 2$ neighboring crystals creates a gap of average thickness $2c_t + 3a_o$ as in the corresponding sketch in Figure 2b. For any fraction t of melted crystals, the probability of an amorphous gap created by the melting of $n \ge 0$ neighboring crystals is

$$p_n(t) = (1 - t)t^n \tag{10}$$

Hence the amorphous thickness distribution that results after a fraction t of the crystals has melted is

$$h(a) = \sum_{n=0}^{\infty} (1 - t)t^n h_n(a) \tag{11}$$

Here $h_n(a)$, with mean $nc_t + (n + 1)a_o$, is the distribution of amorphous thicknesses resulting from the melting of n neighboring crystals. Each $h_n(a)$ is given by the convolution integral

$$h_n(a) = \underbrace{H_t(c)*H_t(c)*\ldots H_t(c)}_{n \text{ times}}*\underbrace{h_o(a)*h_o(a)*\ldots*h_o(a)*h_o(a)}_{n+1 \text{ times}} \tag{12}$$

This method was described earlier for a simpler model,[27] in which sequential melting is independent of crystal thickness.

Returning to the present work, the $h_n(a)$ terms are not evaluated, but the Fourier theorem is used to calculate the Fourier transform of eq 12:

$$F_{an} = F_{ct}{}^{n} F_{ao}{}^{n+1} \tag{13}$$

where F_{ct} is the Fourier transform of $H_t(c)$ (evaluated numerically) and F is the Fourier transform of $h_o(a)$ (analytical; see eq 7). With eq 13 and eq 11 we get the desired F_a for evaluating the intensity with eq 6:[36]

$$F_a = \sum_{n=0}^{\infty} (1-t) t^n F_{ct}{}^{n} F_{ao}{}^{n+1} = \frac{(1-t)F_{ao}}{1 - tF_{ct}F_{ao}} \tag{14}$$

Should the distribution $h(a)$ itself be needed, it can be obtained by the inverse Fourier transform of F_a. An example is given in Figure 6b, again for the case of original crystallinity $\varphi_o = 0.75$ and for $t = 0.6$. Note particularly that the most probable value of a is unchanged by sequential melting and that the amorphous distribution function $h(a)$ is broadened and positively skewed with subsidiary maxima at increasing values of a corresponding to $n = 1$, $n = 2$, etc.

Next are summarized the analytical expectations of sequential melting. Any extent of melting t results in a mean *transformed* (melted) crystal size $\bar{c}_t$ and a mean *untransformed* (unmelted) crystal size $\bar{c}$ that are related by $t\bar{c}_t + (1-t)\bar{c} = c_o$. Note that as $t \rightarrow 1$, $\bar{c}_t$ approaches c_o and $\bar{c}$ diverges, while the variance σ_c^2 approaches zero. Over the same interval both the average amorphous thickness $\bar{a}$ and variance σ_a^2 diverge. The following relations apply for all values of t:

$$\bar{c} \text{ from } H(c) \text{ and } \bar{c}_t \text{ from } H_t(c) \tag{15a}$$

$$\bar{a} = a_o + (a_o + c_t)\frac{t}{1-t} \tag{15b}$$

$$\bar{x} = \bar{c} + \bar{a} \tag{15c}$$

$$\varphi = \bar{c}/\bar{x} \tag{15d}$$

$$Q \propto \varphi(1-\varphi) \tag{15e}$$

$$K_p \propto N = N_o(1-t) \tag{15f}$$

At issue is the relation between SAXS-derived quantities and the expressions in eq 15. Invariant Q and Porod constant K_p are followed exactly during sequential melting. But the apparent period, phase thicknesses and crystallinity from SAXS bear little relation to the values average values in eq 15, parts a−d.

Sequential melting of a lamellar stack with initial crystallinity $\varphi_o = 0.75$ is presented in Figures 7−9; comparison to Figures 3−5 shows substantial differences from surface melting. The overall intensity distribution in Figure 7 shifts to lower s_1; there appears a dominant contribution at $s_1 = 0$, while the interference maximum weakens and shifts a little below $s_1 = 1$ before being replaced by the monotonic scattering. This is because sequential melting to fraction $t > 0.1$ creates a sensible number of large amorphous gaps (see Figure 6b) that give rise to corresponding large interface separations that in turn cause the intensity to grow at $s_1 < 1$. However, the interference maximum remains near $s_1 = 1$, even though the average period within the partially melted stack has increased for instance to $\bar{x} = 1.7$ for $t = 0.4$ (see Table 2). The reason for this apparent discrepancy is that the most probable amorphous and crystalline sizes remain a_o and c_o, respectively; "diffraction" at $s_1 \approx 1$ occurs from the unmodified parts of the lattice ($n = 0$ in Figure 2b) where the average period is still x_o. For $t > 0.5$, the most probable crystal thickness increases somewhat (see Figure 6a), as does the most probable period x_{mp}. However, for this extent of transformation, the one-dimensional lattice is nearly destroyed, and the scattering approaches that for isolated lamellar crystals. The inset in Figure 7 is $I(s_1)$ for $t = 0.9$ and for single particle scattering from lamellae of the same thickness $\overline{c^2} = 1.19$ (increased from $\overline{c_o^2} = 0.56$ in the unmelted stack). Intensity for the single particle calculation is about 10% larger because there each particle scatters independently, while there are still some weak interparticle correlations within the stack melted sequentially to $t = 0.9$ with remaining crystalline fraction $\varphi = 0.11$. Aside from that, the shapes of the two curves are essentially identical, demonstrating conclusively that sequential melting causes the scattering to evolve to a single particle pattern. A related feature is that the crystalline distribution $H(c)$ is narrowed as sequential melting proceeds, so the scattering for $t \rightarrow 1$ is for uncorrelated lamellae with virtually the same thickness.

The correlation functions in Figure 8 reflect the same behavior, with a small shift of the maximum in $\gamma(r)$ to larger r for $t \leq 0.4$. Yet more melting results in a correlation function without a detectible maximum. At the same time, the first minimum in $\gamma(r)$ is suppressed because of increased intensity at low s_1.[27] Sequential melting to $t = 0.9$ (crystallinity $\varphi = 0.11$) results in $\gamma(r)$ that decreases linearly to zero at $r = \bar{c} = 1.09$, as expected for single particle scattering.

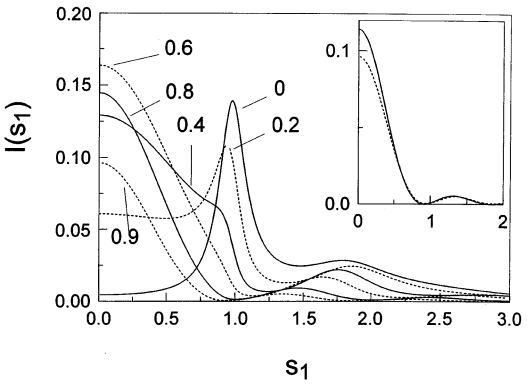

Figure 7. Intensity $I(s_1)$ for sequential melting of stack with initial crystallinity $\varphi_o = 0.75$ for transformed fractions t as indicated. The insert compares $t = 0.9$ stack (- -) with single particle scattering (—).

Table 2. Sequential Melting for Lattice with Initial Crystallinity $\varphi_0 = 0.75$

t	$\bar{x}$	x_{mp}	L_B	L_γ	L_G	φ	$\varphi_{\gamma 0}$	$\varphi_{\gamma min}$	φ_G
0	1.00	1.00	1.02	1.02	1.01	0.75	0.72	0.75	0.75
0.2	1.24	1.00	1.07	1.08	1.03	0.66	*c*	0.87	0.73
0.4	1.70	1.00	1.11	1.16	1.08	0.52	*c*	0.92	0.69
0.6	2.43	1.03	*b*	(1.25)	1.15	0.38	*c*	(0.95)	0.65
0.8	5.08	1.15	*b*	(1.39)	1.25	0.20	*c*	(0.98)	0.60
0.9	10.38	1.24	*b*	(1.57)	(1.32)	0.11	*c*	*b*	(0.57)

[a] Values in parentheses indicate a shallow maximum in $\gamma(r)$ or a minimum in $G(r)$ that is too weak to be seen in real experimental data. [b] No perceptible maximum in $I(s_1)$ or minimum in $\gamma(r)$. [c] Equation returns a complex result.

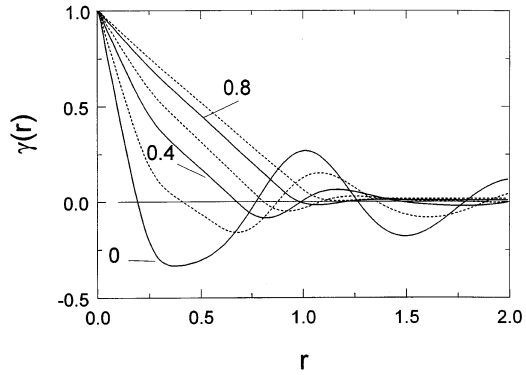

Figure 8. Correlation function $\gamma(r)$ for sequential melting of stack with initial crystallinity $\varphi_o = 0.75$. Solid lines have t as indicated, while dashed lines are for $t = 0.2$, 0.6, and 0.9.

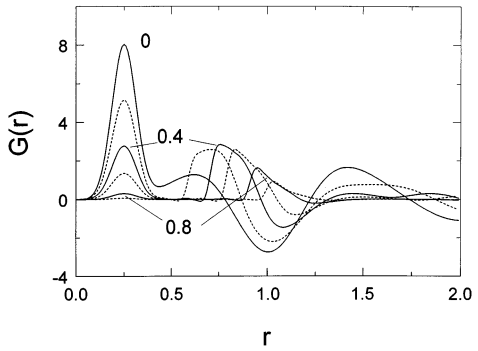

Figure 9. Interface distribution function $G(r)$ for sequential melting of stack with initial crystallinity $\varphi_o = 0.75$. Solid lines have t as indicated, while dashed lines are for $t = 0.2$, 0.6, and 0.9.

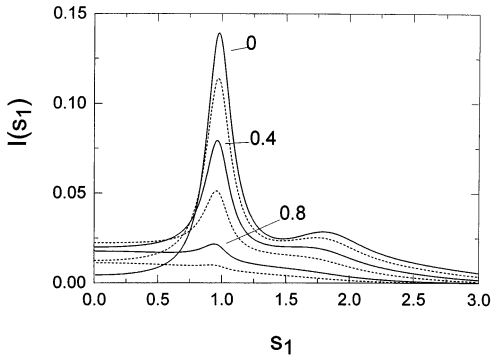

Figure 10. Intensity $I(s_1)$ for sequential melting of stack with initial crystallinity $\varphi_o = 0.25$. Solid lines are for transformed fractions t as indicated, while dashed lines are for $t = 0.2$, 0.6, and 0.9.

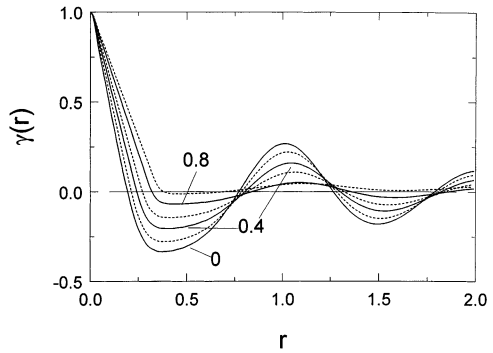

Figure 11. Correlation function $\gamma(r)$ for sequential melting of stack with initial crystallinity $\varphi_o = 0.25$. Solid lines have t as indicated, while dashed lines are for $t = 0.2$, 0.6, and 0.9.

Dimensions from $I(s_1)$ and $\gamma(r)$ are presented in Table 2, along with average period $\bar{x}$, most probable period x_{mp} and actual crystallinity φ of the partially melted lattice. The intensity and correlation function estimates L_B and L_γ are seen to reflect x_{mp}, although they are distorted by the monotonic scattering. This monotonic aspect to the pattern makes crystallinity estimates $\varphi_{\gamma 0}$ and $\varphi_{\gamma min}$ virtually worthless. The reader may wonder why stack crystallinity when $t = 0.9$, for example, is 0.11, not $\varphi_o(1 - t) = 0.075$. The reason is sequential melting proceeds with the thinnest crystals first, so the correct definition $n = \bar{c}/\bar{x}$ (eq 15d) is 0.11 in this case.

The behavior of the interface distribution function in Figure 9 is quite instructive. Consider first the peak at $r = 0.25 = a_o$ that corresponds to the amorphous distribution $h(a)$. With increased sequential melting this portion of $G(r)$ becomes weaker because $h(a)$ broadens and the maximum at a_o is reduced (see Figure 6b). Simultaneously, the crystalline distribution $H(c)$ narrows and shifts to larger values, which accounts for the modified shape of $G(r)$ for $r > 0.5$. These crystalline peaks in $G(r)$ are positively skewed, as is the shape of $H(c)$ in Figure 6a. The location of the minimum in $G(r)$, which gives the average period L_G, drifts to larger values and it is somewhat greater than x_{mp}. L_G is observable for $t = 0.6-0.8$, whereas interference effects for those structures are not evident in either $I(s_1)$ or $\gamma(r)$. Apparent crystallinity φ_G remains near $\varphi_o = 0.75$ because the interface distribution function reflects most probable lengths. For $t = 0.9$ the only feature in $G(r)$ is the crystalline peak at $r > 1$, consistent with the notion that the structure is essentially isolated lamellae. It should be noted that $G(r)$ weakens as $t \rightarrow 1$ with sequential melting because the number of lamellae $N = N_o(1 - t)$ approaches zero. With surface melting, on the other hand, N remains at N_o and $G(r)$ is not suppressed, as seen in Figure 5.

Sequential melting of a stack with low initial crystallinity $\varphi_0 = 0.25$ is considered in Figures 10−12. While intensity at $t = 0$ is identical to that of the $\varphi_o = 0.75$ lattice in Figure 7 because of Babinet reciprocity, melting effects when $t > 0$ appear more moderate with the lower crystallinity stack. The reason for this is straightforward; consider the case when $t = 0.4$, meaning that 40% of the crystals initially present have melted. This phase transition applies to approximately $t\,\varphi_o$ of the lattice, actually 8% of the stack for $\varphi_o = 0.25$, as opposed to the larger 23% of the stack for $\varphi_o = 0.75$. Sequential melting of the low crystallinity stack results in a steady decrease in peak and integrated intensities while the pattern acquires more monotonic character. Because the monotonic scattering is less dominant, one observes the interference maximum near $s_1 \approx 1$ even when $t = 0.9$.

The correlation functions in Figure 11 are well behaved; all features shift systematically with increased sequential melting, and a maximum corresponding to L_γ is apparent even for $t = 0.9$. The interface distribution function shows the low r peak corresponding to $H(c)$ that shifts to larger distances as melting proceeds. Perhaps unexpected is the lack of a minimum to give L_G for $t = 0.8$ and 0.9; recall that interference effects are seen in both $I(s_1)$ and $\gamma(r)$. In $G(r)$, however, the second positive peak corresponding to amorphous $h(a)$ is shifted into the range of the most probable stack period near $r = 1$, effectively counteracting the long period minimum.

Table 3. Sequential Melting for Lattice with Initial Crystallinity $\varphi_0 = 0.25$[a]

t	$\bar{x}$	x_{mp}	L_B	L_γ	L_G	φ	$\varphi_{\gamma 0}$	$\varphi_{\gamma min}$	φ_G
0	1.00	1.00	1.02	1.00	1.01	0.25	0.28	0.25	0.25
0.2	1.24	1.00	1.04	1.03	1.02	0.22	0.29	0.22	0.25
0.4	1.70	1.00	1.04	1.05	1.04	0.17	0.36	0.17	0.26
0.6	2.43	1.03	1.05	1.07	1.07	0.13	*b*	0.13	0.27
0.8	5.08	1.15	1.06	1.09	(1.11)	0.07	*b*	0.06	(0.30)
0.9	10.38	1.24	1.07	1.13	(1.08)	0.04	*b*	0.01	(0.32)

[a] Values in parentheses indicate a shallow minimum in $G(r)$ that is too weak to be seen in real experimental data. [b] Equation returns a complex result.

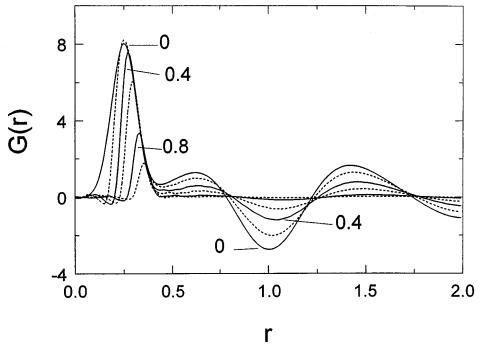

Figure 12. Interface distribution function $G(r)$ for sequential melting of stack with initial crystallinity $\varphi_o = 0.75$. Solid lines have t as indicated, while dashed lines are for $t = 0.2$, 0.6, and 0.9.

Dimensions and crystallinities are given in Table 3. Note that average $\bar{x}$ and most probable x_{mp} periods have the same dependence on fractional melting t as in the $\varphi_o = 0.75$ case in Table 2. But the smaller monotonic scattering makes pattern analysis more meaningful in some ways. It was mentioned above that periods L_B and L_γ are perceptible up to $t = 0.9$, although neither of these quantities is close to the average period $\bar{x}$. Apparent phase fraction $\varphi_{\gamma min}$ is remarkably accurate in this example, although the companion $\varphi_{\gamma 0}$ is unreliable. The interface distribution function, responding again to most probable values, maintains φ_G near 0.25.

Two prominent results follow from this modeling study of sequential melting. First, the apparent period L from any analysis of the scattering pattern remains near the original value x_o even though the average $\bar{x}$ increases from 1 to about 5 for $t = 0.8$. Second, sequential melting destroys the periodicity of the stack, so that the scattering pattern at the final stages of melting ($t \rightarrow 1$) is for isolated lamellar crystals. The conversion from peaked to monotonic patterns is more rapid for stacks with large initial crystallinity. Certain of these features have been found in simpler treatments of sequential melting by Fischer et al.[37] and by Crist,[27] and were considered in a qualitative fashion by Schultz et al.[38]

Stack Melting

As different complete stacks melt, the structure fraction φ_{st} decreases, while the internal structure of surviving stacks is unchanged. This mechanism is illustrated in Figure 13 with a simple model composed of stacks with five values of $\bar{x} = 1.0$, 0.80, 0.67, 0.57, and 0.50 that are present in relative amounts of 0.5, 0.72, 1, 1 and 1, respectively. Crystallinity of each stack is $\varphi = 0.5$, and $g_x = 2$ as before. Intensity for the entire system ($t = 0$) displays weak maxima corresponding to the four largest values of $\bar{x}$ that are artifacts of the coarseness of the discrete distribution. Relative stack populations were chosen to give an overall maximum at $s_1 \approx 1.5$.

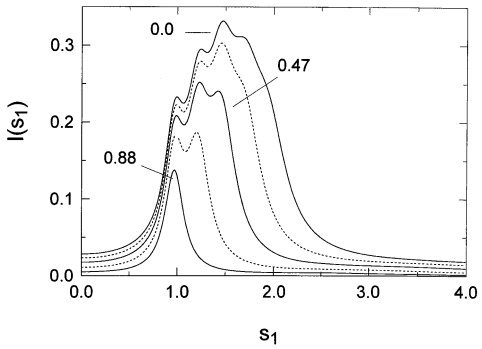

Figure 13. Intensity for a discrete distribution of 5 stacks with different $\bar{x}$ ranging from 0.5 to 1. Stack melting according to increasing period results in intensities corresponding to different values of t. Solid lines are for values indicated, while dashed lines are for $t = 0.24$ and $t = 0.71$.

Melting is simulated by sequentially removing the stack population with the smallest period. As every lamella in a stack with a particular $\bar{x}$ melts at once, the variance of $H(c)$ within each stack is implicitly very small. SAXS accompanying stack melting has two very characteristic features; the maximum is moved to smaller values of s_1, and the intensity steadily decreases. The latter would occur regardless of the local crystallinity φ of any stack or stacks; melting proceeds only by reducing φ_{st}. In the present example, the apparent period L_B increases from 0.67 to 1, a 50% change that is seen in many experiments. While this model captures the shift of peak position to lower s_1 during melting (see Figure 1a), it does not generate monotonic intensity at small s_1. In the interest of space, the correlation functions and interface distribution functions are not presented.

Discussion and Conclusions

Following a summary of SAXS characteristics of the three melting mechanisms, these features will be compared to those observed in experiments. Except as noted, intensity changes, either at specific s_1 or integrated, do not include increases of about 30%/100 °C from $\Delta\rho_e^2(T)$. *Surface melting* occurs at constant period L, and without any increase in intensity at low s_1. Peak or integrated intensity will go through a maximum at $\varphi = 0.5$ if the original stack crystallinity φ_o is greater than 0.5. Otherwise, intensity decreases continuously to zero. Taken literally, surface melting preserves all stacks until melting is complete at $t = 1$, hence the Porod constant (eq 9) should remain constant throughout the melting process, then abruptly fall to zero when $t = 1$. *Sequential melting* also occurs with apparent period L nearly constant, even though the true average periodicity $\bar{x}$ is roughly proportional to $1/(1 - t)$, diverging as t approaches 1. In contrast to surface melting, low s_1 intensity increases substantially during sequential melting, and the process ends with scattering from the most stable (thickest) isolated lamellae. As lamellae are removed from the stack, the Porod constant K_p decreases throughout sequential melting. Integrated intensity Q may go through a maximum if $\varphi_o > 0.5$, but the interference peak decreases steadily (see Figure 7 and Figure 10). *Stack melting* is the only mechanism of the three that may proceed with a substantial increase

in apparent period L. With this process $Q(T)$ will always decrease, regardless of initial crystallinity, as the local stack φ of surviving stacks is unchanged by this sort of melting. Here, as with surface melting, there is no growth of intensity at low s_1, and, as with sequential melting, K_p continuously decreases to zero.

How do these different SAXS/melting behaviors compare to experiment? The melting of the PEN(b) crystallized at a relatively high $T_c = 240$ °C (Figure 1b) is consistent with sequential melting. The position of the interference peak is nearly constant, the peak intensity drops, and low s intensity increases. Similar behavior has been reported very rarely; once for poly(ethylene oxide) single crystals,[24] and more recently for poly(ethylene terephthalate) that had been isothermally crystallized at 231 °C for 72 h.[39] Intensity curves were not published for the PET study, but melting occurred at nearly constant period L_γ and phase thicknesses l_1 and l_2. Recall that most probable dimensions are fixed (or nearly so) during sequential melting. The PEN and PET samples in question had been crystallized at relatively small undercoolings, and the lamellar crystals were presumably thick and resistant to rearrangement by either melting and recrystallization or by thickening during the melting process. No information whatever was given for the PEO crystals.

The more common SAXS/melting behavior exemplified by Figure 1a fits none of the three models considered here. The conspicuous shift of the interference peak to lower s is consistent with stack melting, but the increased peak intensity is not (see Figure 13). Given that crystals formed at low $T_c = 165$ °C in this instance are unstable, melting and recrystallization and/or lamellar thickening are likely responsible for most of the SAXS effects. Indeed, Denchev et al.[13] suggest this sort of process, in part to explain the fact that L_γ for PEN(a) exceeds that of PEN(b) before final melting.

It is not the purpose of this paper to identify the mechanism or mechanisms by which specific polymers melt. Qualitative evidence has been presented for sequential melting in three cases, two of which involve relatively stable crystals formed from the melt at low undercooling. The majority of cases, represented by Figure 1a, are not understood. Basal surface melting is impossible here. The patterns have some characteristics of stack melting, but intensity changes suggest reorganization by some means. Evolution of the pattern from peaked to monotonic implies that something akin to sequential melting occurs in the final stages (see below). While SAXS is undisputably a valuable technique for monitoring structure during polymer melting (and crystallization), certain points deserve more consideration than normally accorded.

First, results from standard analyses of $\gamma(r)$ or $G(r)$ to estimate phase dimensions may be incorrect or misleading. Correlation function measures of l_2 (and hence φ) are both insensitive and unreliable for stacks with $0.4 < \varphi < 0.6$. Structural disorder within a stack and/or monotonic scattering often cause $\varphi_{\gamma 0}$ to be *too close to* 0.5 (either too large or too small), while physically impossible (complex) values are returned when $\varphi = 0.5 \pm 0.1$.[26] Examples can be seen in Tables 1−3. For the other method of estimating stack crystallinity, both stack disorder and monotonic scattering cause the minimum in $\gamma(r)$ to be shallower; hence, $\varphi_{\gamma\min}$ is *too far from* 0.5, particularly when $\varphi = 0.5 \pm 0.1$. An interesting case is sequential melting of the $\varphi_o = 0.25$ stack (Table 3), where $\varphi_{\gamma\min}$ is an excellent measure of the true crystalline fraction $\varphi = \bar{c}/\bar{x}$. However, the apparent crystalline thickness $l_2 = \varphi_{\gamma\min} L_\gamma$ *decreases* from 0.25 to 0.07 for sequential melting to $t = 0.8$, while the actual average crystal thickness $\bar{c}$ *increases* from 0.25 to 0.36. Hence the correlation function would give a badly misleading impression of the structural changes taking place, in this case because the stack crystallinity is based on average quantities, while the period L_γ is close to the most probable value. A quite different story is conveyed by the interface distribution function $G(r)$ over the same interval. While the true stack crystallinity drops to $\varphi = 0.13$ for $t = 0.6$, the apparent crystallinity φ_G is essentially constant near $\varphi_o = 0.25$; this sort of "misinformation" could seriously impair interpretation of the melting process. Here the apparent crystal size $l_2 = \varphi_G L_G$ increases from 0.25 to 0.29, which reasonably approximates the upward drift of $\bar{c}$ to 0. 32 over the same melting range. Other examples could be given; these all reflect difficulties that arise from extracting dimensions by direct inspection, particularly when strongly skewed distribution functions are present.

The second issue deals with monotonic scattering. Close inspection reveals that $\gamma(r)$ or $G(r)$ analyses are often *not* made throughout the entire melting process. Patterns such as the apparently monotonic one for PEN(a) at 262 °C (Figure 1a) are ignored, except for integration to obtain $Q(T)$.[13] For this sample the SAXS pattern was not analyzed between 255 and 274 °C, which is exactly the range over which the invariant $Q(T)$ decreased from its maximum value to zero, and clearly where the majority of the melting occurred. Overlooking or ignoring monotonic patterns will cause one to miss the single lamellae scattering that characterizes the end of melting. An instructive example in which the "monotonic" curves observed at the highest temperatures were analyzed is provided by Rule and Liggat.[17] Heating poly(3-hydroxybutyrate) to 170 °C causes L_B to increase by over four times to 30 nm at $T = 170$ °C—the pattern has an interference maximum. In the remaining interval before final melting at 180 °C, the pattern becomes monotonic, indicating that isolated lamellae with thickness $c \approx 10$ nm are the last to melt.

This work is concluded with a number of suggestions to further our understanding of polymer melting. The shape and intensity of the scattering pattern conveys information on the melting process that, at a minimum, complements the dimensions extracted from $\gamma(r)$ or $G(r)$. Heat/cool cycles can help clarify which structural changes are reversible and irreversible. Beyond the direct inspection of curves for "average" dimensions, model fitting to the complete curves, as done by Fulcher et al.[24] for $\gamma(r)$ and by Wang et al.[40] for $G(r)$, can provide additional insights. Intensity curves $I(s_1)$ were fitted by Ivanov[41] et al. during the partial melting (up to $t = 0.65$) of poly(tetramethyene terephthalate). Results of that analysis are interpreted to show preferential melting of thin crystals that are neighbored by small amorphous layers, a sort of nonrandom sequential melting with similarities to an earlier model of Strobl et al.[42]

It is doubtful that scattering studies, no matter how detailed or sophisticated, can unravel all the changes taking place during polymer melting. Microscopy can be an invaluable supplement. With transmission electron microscopy, Kanig long ago presented direct evidence for both whole stack melting and intrastack melting in polyethylene.[43] Latimer et al.[44] studied poly-

(aryl ether ether ketone), PEEK. Most important were images of physically separated stacks having lamellae of different thickness, plus the direct observation of stack melting followed by recrystallization. More recently, Liu et al. have followed the melting of spherulites in thin films of isotactic polystyrene.[45] Structural changes included fragmentation of originally wide lamellae, and an increase in the most probable amorphous layer thickness. As with Kanig's study, images for appreciable melting ($t \rightarrow 1$) are of largely uncorrelated lamellae, consistent with single lamellae scattering described above. High-temperature atomic force microscopy can reveal changes occurring over time. Beekmans et al.[46] observed lamellae (or lamellar stacks) in poly(ethylene oxide) spherulites to shrink in the long (radial) direction when heated into the melting range. Zhou et al.[47] studied single crystals of syndiotactic polypropylene grown from the melt. Here melting started at the long edges of sectorized lamellae, then went to all edges at a higher temperature. Linear low-density polyethylene, which resembles a random copolymer, was considered by Godovsky and Magonov.[48] They found that partial melting below 85 °C was accomplished by the removal of thin (secondary) lamellae. Heating to 90 °C caused melting and recrystallization to occur. It is likely that the most successful studies of polymer melting will combine SAXS and appropriate microscopies.

References and Notes

(1) von Rossem, L. A.; Lotichius, J. *Rubber Chem. Technol.* **1929**, *2*, 378.
(2) Flory, P. J. *J. Chem. Phys.* **1949**, *17*, 223.
(3) Wunderlich, B. *Macromolecular Physics*; Academic Press: New York, 1980; Vol. 3, p 30 ff, p 135 ff.
(4) Crist, B.; Mirabella, F. M. *J. Polym. Sci., Part B: Polym. Phys.* **1999**, *37*, 3131.
(5) Belbéoch, B.; Guinier, A. *Makromol. Chem.* **1959**, *31*, 1.
(6) O'Leary, K.; Geil, P. H. *J. Macromol. Sci.—Phys.* **1967**, *B1*, 147.
(7) Pope, D. P.; Keller, A *J. Polym. Sci.: Polym. Phys. Ed.* **1976**, *14*, 821.
(8) Fischer, E. W. *Pure Appl. Chem.* **1971**, *26*, 385.
(9) Ruland, W. *Colloid Polym. Sci.* **1977**, *255*, 417.
(10) Goderis, B.; Reynaers, H.; Koch, M. H.; Mathot, V. B. F. *J. Polym. Sci., Part B: Polym. Phys.* **1999**, *37*, 1715.
(11) Porod, G. In *Small Angle X-ray Scattering*, Glatter, O.; Kratky, O., Eds.; Academic Press: New York, 1982; Chapter 2.
(12) Roe, R. J. *Methods of X-ray and Neutron Scattering in Polymer Science*; Oxford University Press: New York 2000; Chapter 5.
(13) Denchev, Z.; Nogales, I.; Šics, I.; Ezquerra, T. A.; Baltá-Calleja, F. J. *J. Polym. Sci., Part B: Polym. Phys.* **2001**, *39*, 881.
(14) Fougnies, C.; Damman, P.; Dosière, M.; Koch, M. H. J. *Macromolecules* **1997**, *30*, 1392.
(15) Vonk, C. G.; Koga, Y. *J. Polym. Sci., Polym. Phys. Ed.* **1985**, *23*, 2539.
(16) Schmidtke, J.; Strobl, G.; Thurn-Albrecht, T. *Macromolecules* **1997**, *30*, 5804.
(17) Rule, R. J.; Liggat, J. J. *Polymer* **1995**, *36*, 3831.
(18) Schultz, J. M.; Lin, J. S.; Hendricks, R. W. *J. Appl. Crystallogr.* **1978**, *11*, 551.
(19) Albrecht, T.; Strobl, G. *Macromolecules* **1996**, *29*, 783.
(20) Akpalu, Y. A.; Amis, E. *J. Chem. Phys.* **1999**, *111* 8686.
(21) Hsiao, B. S.; Gardner, K. H.; Wu, D. Q.; Chu, B. *Polymer* **1993**, *34*, 3996.
(22) Denchev, V.; Nogales, A.; Ezquerra, T. A.; Fernandes-Nascimento, J.; Balta-Calleja, F. J. *J. Polym. Sci., Part B: Polym. Phys.* **2000**, *38*, 1167.
(23) Vonk, C. G.; Kortleve, G. *Kolloid Z. Z. Polym.* **1967**, *220*, 19.
(24) Fulcher, K. U.; Brown, D. S.; Wetton, R. E. *J. Polym. Sci.: Part C* **1972**, *38*, 315.
(25) Ruland, W. *Colloid Polym. Sci.* **1977**, *255*, 417.
(26) Crist, B. *J. Macromol. Sci.—Phys.* **2000**, *B39*, 493.
(27) Crist, B. *J. Polym. Sci., Part B.: Polym. Phys.* **2001**, *39*, 2454.
(28) Wang, Z.-G.; Hsiao, B. S.; Fu, B. X.; Liu, L.; Yeh, F.; Sauer, B. B.; Chang, H.; Schultz, J. M. *Polymer* **2000**, *41*, 1791.
(29) Albrecht, T.; Strobl, G. *Macromolecules* **1995**, *28*, 5827.
(30) Goderis, B.; Peeters, M.; Mathot, V. B. F.; Koch, M. H. J.; Bras, W.; Ryan, A. J.; Reynaeers, H. *J. Polym. Sci., Part B: Polym. Phys.* **2000**, *38*, 1975.
(31) Verma, R. K.; Hsiao, B. S. *Trends Polym. Sci.* **1996**, *4*, 312.
(32) Verma, R. K.; Velikov, V.; Kander, R. G.; Marand, H.; Chu, B.; Hsiao, B. S. *Polymer* **1996**, 5357.
(33) Hermans, J. J. *Recueil Trav. Chem. Pays-Bas* **1944**, *63*, 5.
(34) Hosemann, R.; Bagchi, S. N. *Direct Analysis of Diffraction by Matter*; North-Holland: Amsterdam, 1962; Chapter 12, pp 408−428.
(35) Nam, J. Y.; Kadomatsu, S.; Saito, H.; Inoue, T. *Polymer* **2002**, *43*, 2101.
(36) A reviewer kindly supplied the closed form of eq 14. Results presented here were obtained using the sum with n up to 70.
(37) Fischer, E. W.; Martin, R.; Schmidt, G. F.; Strobl, G. Presented at the IUPAC International Symposium on Macromolecular Chemistry, Toronto, Canada, 1968; Paper A6.17.
(38) Schultz, J. M.; Fischer, E. W.; Schaumburg, O.; Zachmann, H. A. *J. Polym. Sci.: Polym. Phys. Ed.* **1980**, *18*, 239.
(39) Wang, Z.-G.; Hsiao, B. S.; Sauer, B. B.; Kampert, W. G. *Polymer* **1999**, *40*, 4615.
(40) Wang, Z.-G.; Hsiao, B. S.; Stribeck, N.; Gehrke, R. *Macromolecules* **2002**, *35*, 2200.
(41) Ivanov, D. A.; Hocquet, S.; Dosière, M.; Koch, J. H. J. *Phys. Rev. B*, in press.
(42) Strobl, G.; Schneider, M.; Voight-Martin, I. *J. Polym. Sci.: Polym. Phys. Ed.* **1980**, *18*, 1361.
(43) Kanig, G. *Colloid Polym. Sci.* **1982**, *260*, 356.
(44) Lattimer, M. P.; Hobbs, J. K.; Hill, M. J.; Barham, P. J. *Polymer* **1992**, *33*, 3971.
(45) Liu, T.; Petermann, J.; He, C.; Liu, Z.; Chung, T.-S. *Macromolecules* **2001**, *34*, 4305.
(46) Beekmans, L. G. M.; van der Meer, D. W.; Vansco, G. J. *Polymer* **2000**, *43*, 1887.
(47) Zhou, W.; Cheng, S. Z. D.; Putthanarat, S.; Eby, R. K.; Reneker, D. H.; Lotz, B.; Magonov, S.; Hsieh, E. T.; Geerts, R. G.; Palackal, S. J.; Hawley, G. R.; Welch, M. B. *Macromolecules* **2000**, *33*, 6861.
(48) Gdovsky, Y. K.; Magonov, S. N. *Langmuir* **2000**, *16*, 3549.

MA030113D